

Chapter 3

A Large Ion Collider Experiment

ALICE (A Large Ion Collider Experiment) is a general-purpose experiment at the CERN LHC [1]. It was conceived and built to focus on the study of QCD and heavy-ion collisions. It is designed to address the physics of strongly interacting matter and the quark-gluon plasma at extreme values of energy density and temperature in nucleus-nucleus collisions. Nonetheless, its physics programme also includes proton-proton and proton-nucleus collisions, which provide reference data for the heavy-ion programme and address a number of specific strong-interaction topics for which ALICE is complementary to the other LHC experiment. During the LHC Long Shutdown 2, between 2019 and 2021, ALICE underwent a major upgrade to improve its capabilities to probe the QGP with heavy-flavour quarks, and to enable completely new measurements of the thermal emission of dielectron pairs [2].

3.1 The Large Hadron Collider

The Large Hadron Collider (LHC) is a two-ring superconducting hadron accelerator and collider based at CERN [3], near Geneva, on the border between Switzerland and France. The LHC is the world’s largest circular particle accelerator with a 26.7-kilometre circumference housed in a 3.8-metre-wide tunnel buried 50 to 175 metres underground, capable of accelerating protons up to energies of $\sqrt{s} = 14$ TeV and heavy ions (e.g., $^{208}\text{Pb}^{82+}$) up to a centre-of-mass energy per nucleon pair of $\sqrt{s_{\text{NN}}} = 5.5$ TeV.

The LHC, which is located in the same tunnel previously used to host the Large Electron-Positron Collider [4] (LEP), is the final stage of a chain of accelerators that provide protons and heavy ions with sufficient energy to be injected into the LHC, illustrated in Fig. 3.1. Protons are firstly collected by stripping electrons from a gaseous hydrogen source with an electric field and then grouped into bunches. The Linear accelerator 4 (Linac 4), the first linear accelerator in the LHC injection chain, accelerates negative hydrogen ions to 160 MeV. The ions are then stripped of their two electrons, and protons are subsequently injected into the Proton Synchrotron Booster (PSB), which accelerates them to 1.4 GeV, and then into the Proton Synchrotron (PS) and the Super Proton Synchrotron (SPS), reaching 25 and 450 GeV, respectively. The protons are finally injected in the LHC, where they are accelerated

up to a maximum energy of 7 TeV. In the LHC, the beams are forced to follow the circular path of the ring by strong magnetic fields (~ 8 T) produced by superconducting dipole magnets. Other magnets are used to steer and focus the beams in the eight different interaction points.

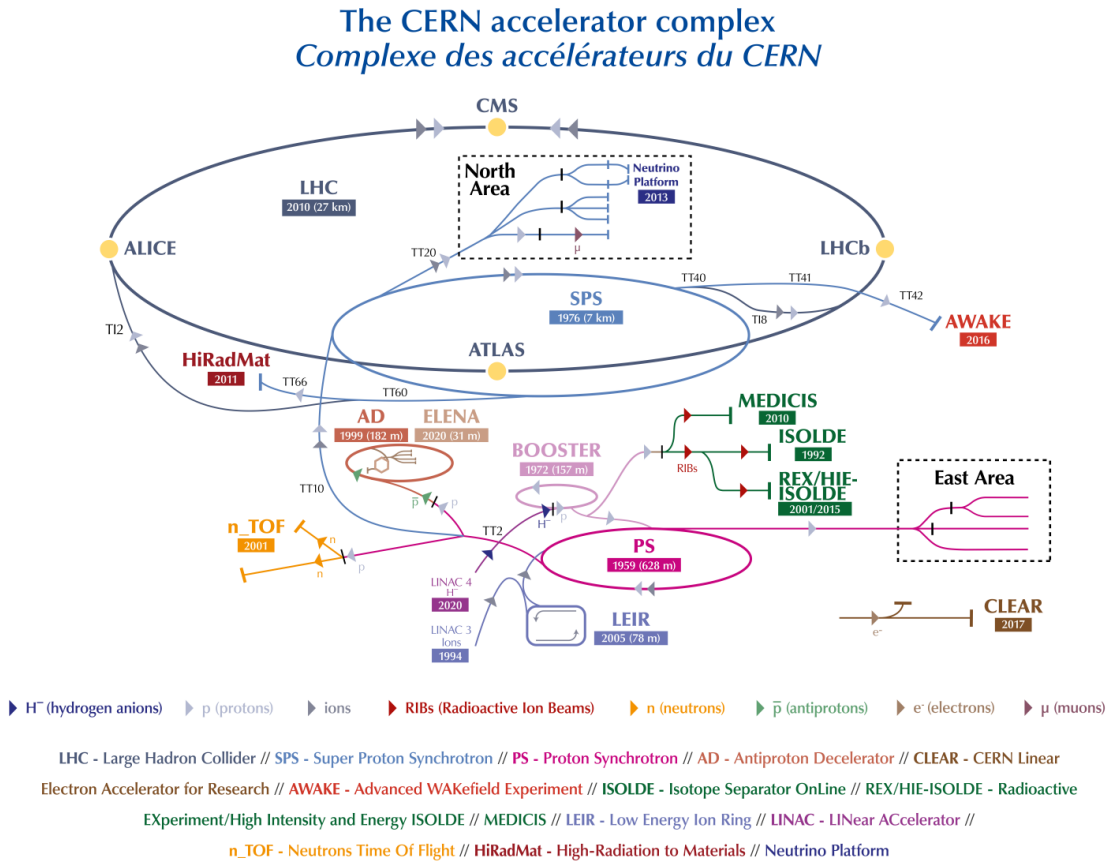


Figure 3.1: The Large Hadron Collider (LHC) accelerator complex at CERN. Figure taken from Ref. [5].

Heavy-ion acceleration follows a similar path. Pb ions ($Pb^{25+} - Pb^{28+}$) are extracted in the Electron-Cyclotron Resonance (ECR), and are focused and accelerated in a Radio-Frequency Quadrupole (RFQ) using only electric fields. Pb^{28+} ions with momentum of $2.5 \text{ keV}/c$ are selected with a spectrometer, and are accelerated to $4.2 \text{ MeV}/c$ in the Linear accelerator 3 (Linac 3). A first $0.5 \mu\text{m}$ copper stripping foil is then used to increase the charge state of the ions to Pb^{53+} . The Low Energy Ion Ring (LEIR) groups the ions into bunches and accelerates them to 72 MeV. The PSB and PS then accelerate the ions to 95.4 MeV and 5.09 GeV. After the PS, a copper stripper ($\sim 1 \text{ mm}$) is used to further ionise the Pb ions to Pb^{82+} , which are then accelerated to 158 GeV in the SPS. The ions are finally injected into the LHC, where they are accelerated up to 2.76 TeV per nucleon.

The LHC can collide protons with protons, protons with heavy ions, and heavy ions with heavy ions. The LHC has four main interaction points, where the four main experiments are located: A Large Ion Collider Experiment (ALICE),

A Toroidal LHC ApparatuS (ATLAS), Compact Muon Solenoid (CMS), and LHC-beauty (LHCb). The four experiments were conceived and built to address different physics topics: ATLAS and CMS are general-purpose detectors designed to study the Higgs boson, which they discovered in 2012 [6, 7] and to search for physics beyond the Standard Model; LHCb is dedicated to the measurement of beauty quarks as proxy for CP violation studies, and to the study of matter-antimatter asymmetry. ALICE is the only detector at the LHC that is dedicated to the study of QCD rather than the electroweak sector of the Standard Model. A detailed description of the ALICE apparatus is given in the following sections.

3.2 The ALICE experiment

The physics programme of ALICE was designed to study the properties of strongly interacting matter at the extreme values of energy density and temperature reached in ultra-relativistic heavy-ion collisions. This unique environment poses several challenges, the most stringent one being the need to carry out measurements in a very high multiplicity environment. Originally, estimates for the charged particle multiplicity density at mid-rapidity in central Pb–Pb collisions ranged from $dN/d\eta = 2000$ up to almost $dN/d\eta = 8000$. Detectors with high granularity, fast readout capabilities, and high radiation hardness were therefore needed. The ALICE detector was designed to meet these requirements, and to provide a comprehensive set of measurements to study the properties of the QGP. The ALICE apparatus is shown in Fig. 3.2. It is based on a central barrel, located inside a magnet which provides a magnetic field of ~ 0.5 T, covering full azimuth ($0 < \varphi < 2\pi$) and the pseudorapidity region $|\eta| < 0.9$, and a forward muon system with a dipole magnet providing a total bending power of $B\rho = 3$ Tm, covering full azimuth and pseudorapidity interval $-4.0 < \eta < -2.5$. The pseudorapidity η is defined from the polar angle θ as $\eta \equiv -\log(\tan(\theta/2))$.

The ALICE coordinate system is a right-handed system with the z -axis pointing along the beam direction, in the direction away from the muon arm, the y -axis pointing vertically up, and the x -axis pointing horizontally towards the center of the LHC. The nominal interaction point is the origin of the coordinate system. The two sides of the apparatus along the beam axis are referred to as the C-side, where the muon arm is positioned, and the A-side, where the FV0 is positioned. The polar angle θ is defined with respect to the z -direction, while the azimuthal angle φ increases counter-clockwise starting from the x -axis towards the CMS side.

The central barrel is enclosed in the L3 solenoid, which has an internal length of 12.1 m and a radius of 5.75 m, providing a magnetic field of 0.5 T. The L3 experiment was a detector at the Large Electron-Positron Collider (LEP) at CERN, which was built in the cavern where ALICE is now located, operating from 1989 to 2000. The central barrel detector system is designed for efficient tracking in the high track-density environment of heavy-ion collisions, covering transverse momenta from ~ 100 MeV/ c to ~ 100 GeV/ c with excellent hadron and electron identification capabilities. It also reconstructs primary and secondary vertices. This allows for precise measurements of ground-state heavy-flavour hadrons, which typically decay at a distance of ~ 100 μ m from the primary vertex. The L3 magnet hosts the Inner Tracking

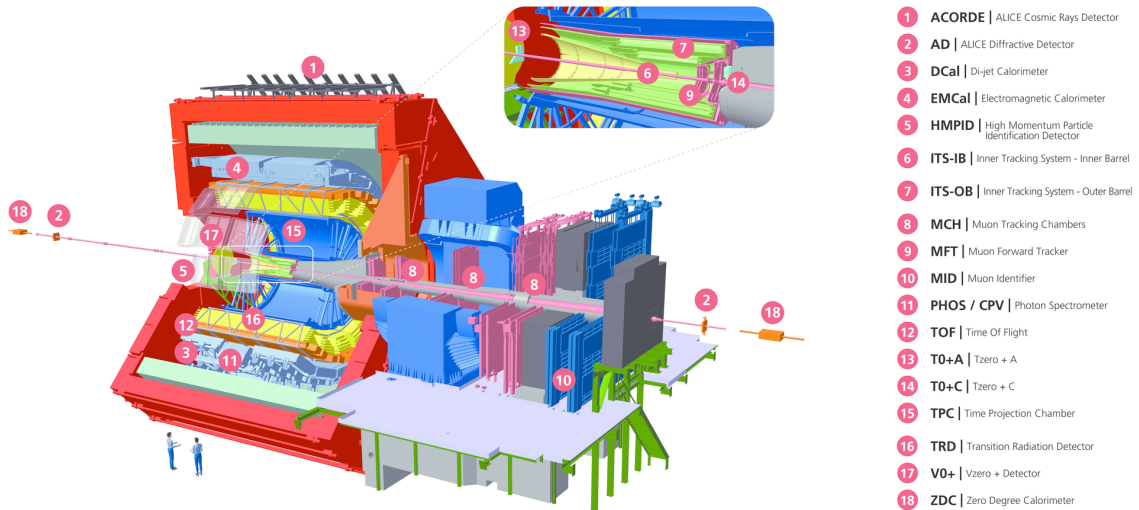


Figure 3.2: The ALICE experimental apparatus. The top right panel shows a zoom of the ITS, FT0-A, FT0-C, and MFT detectors. Figure taken from the ALICE figure repository [8].

System (ITS), the Time Projection Chamber (TPC), the Transition Radiation Detector (TRD), the Time-Of-Flight (TOF) detector, the High-Momentum Particle Identification Detector (HMPID), the ElectroMagnetic Calorimeter (EMCal), and the PHOton Spectrometer (PHOS). The central barrel also includes forward detectors such as the Muon Forward Tracker (MFT) and the Fast Interaction Trigger (FIT). The muon arm covers the forward pseudorapidity range $-4.0 < \eta < -2.5$ and consists of absorbers, a large dipole magnet, planes of triggering Resistive Plate Chambers (RPC) and tracking MultiWire Proportional Chambers (MWPC).

In the following sections, the main components of the ALICE experiment used for the measurements presented in this Thesis are described in detail, ordered from the innermost layer to the outermost detector, following the path of a particle produced in a hadronic collision at mid-rapidity. The upgrades of the ALICE detectors during the LHC Long Shutdown 2 will be highlighted.

3.2.1 ALICE upgrades overview

The ALICE detector underwent a major upgrade during the LHC Long Shutdown 2, between 2019 and 2021, which renewed the experiment, now referred to as ALICE 2. The upgrade aimed at significantly improving the capabilities of ALICE to probe the QGP with heavy-flavour quarks, and enabling new measurements of the thermal emission of dielectron pairs. To achieve these goals, the ALICE detector was improved by enhancing the tracking capabilities of the central barrel detectors and increasing the readout rate of the detectors to collect larger data samples.

The Inner Tracking System (ITS) was replaced with a new detector, the ITS 2, a thinner and lighter detector with the first layer closer to the interaction point, which improves the pointing resolution up to a factor of 3 in the transverse direction and a factor 5 in the longitudinal direction as compared to the old ITS, which operated from 2009 to 2018, as shown in Fig. 3.3.

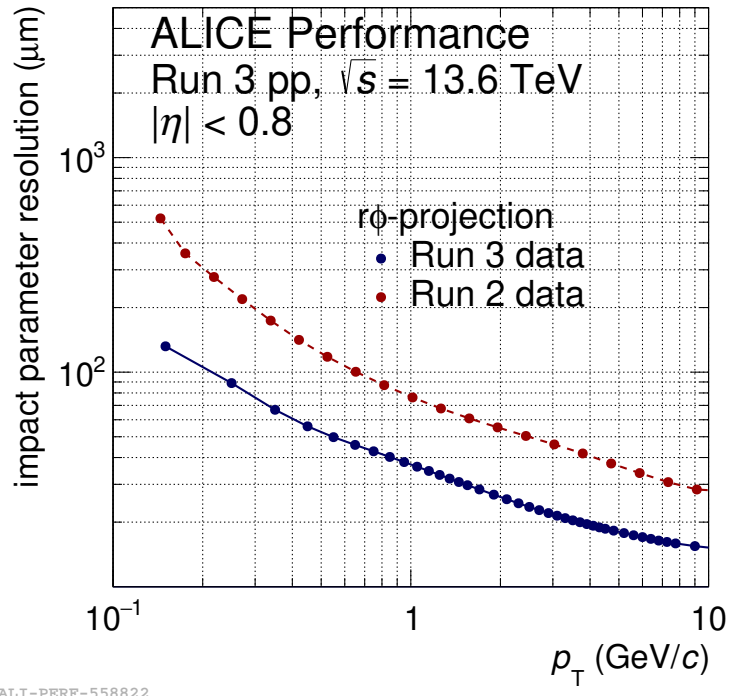


Figure 3.3: Impact parameter resolution in $r\phi$ as a function of p_T in pp collisions at $\sqrt{s} = 13.6 \text{ TeV}$ from Run 3 data compared with the same quantity measured in collisions at $\sqrt{s} = 13 \text{ TeV}$ from Run 2 data. Figure taken from ALICE figure repository [8].

The upgrade strategy for the enhanced readout rate is based on the LHC plans to increase the luminosity of Pb–Pb collisions progressively after the LHC Long Shutdown 2, eventually reaching an interaction rate of about 50 kHz (from less than 1 kHz during LHC Run 1 and Run 2 data-taking periods), i.e. instantaneous luminosity of $\mathcal{L} = 6 \times 10^{27} \text{ cm}^{-2} \text{ s}^{-1}$. At these high interaction rates, each TPC drift time period of $\sim 100 \mu\text{s}$ will contain on average 5 Pb–Pb events. It was therefore decided to use a continuous, untriggered readout strategy. With the MWPC used in ALICE 1 for the TPC readout, the ion backflow into the drift region was suppressed by active gating, limiting the readout rate to about 700 Hz for Pb–Pb collisions. This is overcome in ALICE 2 by using a readout based on Gas Electron Multiplier [9] (GEM) foils, which reduces the ion backflow and resulting space charge in the TPC to a level that can be corrected for while operating the detector with Pb–Pb interaction rates up to 50 kHz.

To synchronise the continuous data stream across all readout and processing branches, the data stream is divided into time frames (TF) of nominal length of 128 LHC orbits ($\sim 11 \text{ ms}$). Each TF is subdivided into heartbeat frames (HBF) with a length corresponding to an orbit of $\sim 89.4 \mu\text{s}$. The detector data are time stamped with a precision of an LHC bunch crossing of 25 ns.

A new software framework has been developed to allow for distributed and efficient processing of this unprecedented amount of data. Because of the continuous

readout in Run 3, the vertex-to-track association is no longer unambiguous. Therefore, in place of the analysis data model used in Runs 1 and 2, based on the hierarchical structure of the "event content", the analysis data model for Run 3 is based on a columnar data format, where collisions and tracks are represented as separate tables, connected by an index. This maps naturally on a "flattened" structure-of-arrays data format. Hence, the columnar data format provided by Apache Arrow [10] was chosen. The new Online-Offline (\mathcal{O}^2) framework ensures a unified and coherent computing environment from data taking up to analysis. Throughout all stages of the data processing, the timeframe represents the minimal processing unit.

The result of asynchronous reconstruction is the Analysis Object Data (AOD) format, with the best calibration available. The content of an AOD timeframe is kept contiguously in shared memory allowing efficient application of parallel execution and pipelining. AODs are stored as ROOT [11] TTrees, exploiting their columnar storage format, and are then used to perform physics analyses.

3.2.2 Inner Tracking System

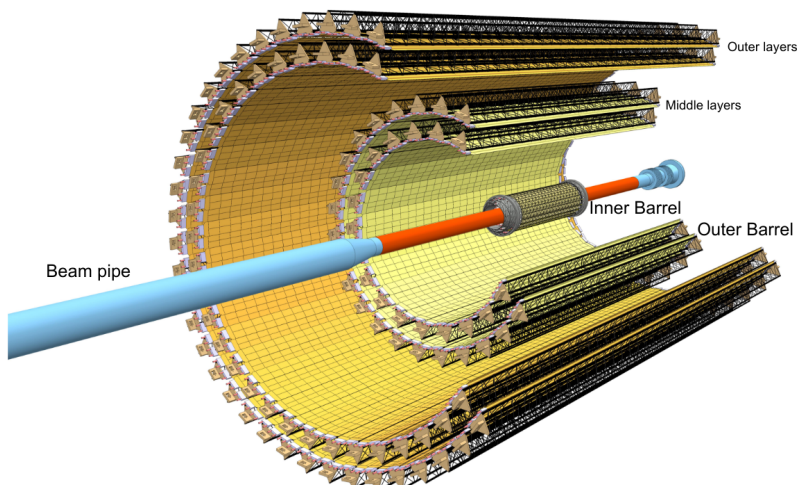


Figure 3.4: Schematic view of the ALICE ITS 2. Figure taken from Ref. [2].

The Inner Tracking System (ITS) is the innermost detector of the ALICE apparatus, and is designed to provide precise tracking and vertexing capabilities in the high-multiplicity environment of heavy-ion collisions. The ITS upgrade is one of the key improvements of the ALICE 2 detector. The ITS 1 was a six-layer silicon detector, with two layers of Silicon Pixel Detectors (SPD), two layers of Silicon Drift Detectors (SDD), and two layers of Silicon Strip Detectors (SSD). The ITS 1 has been replaced by the ITS 2, which is fully constructed with ALPIDE [12] chips, i.e., Monolithic Active Pixel Sensors [13] (MAPS) implemented in a 180 nm CMOS technology for imaging sensors provided by TowerJazz [14].

MAPS are an evolution of the hybrid pixel sensors which have been widely used in the past by several experiments [1, 15, 16, 17]. Hybrid pixel sensors are made of an active layer, typically made of silicon, and a readout layer with the front-end electronics, connected to the active layer with bump-bonds. On top of being

expensive and complex, the bump-bonding operation introduces additional material in the detector, therefore increasing the material budget of the detector. MAPS, on the other hand, are monolithic sensors, where the active layer and the front-end electronics are integrated into the same silicon wafer. This significantly reduces the material budget of the detector. The ALPIDE chip is a $15\text{ mm} \times 30\text{ mm}$ chip, with a pixel size of $29.24\text{ }\mu\text{m} \times 26.88\text{ }\mu\text{m}$, and a total of 512×1024 pixels. Each pixel cell contains a sensing diode, a front-end amplifier, a shaping stage, a discriminator, and a digital section. The digital section includes a multi-event buffer with three hit storage registers and a pixel mask register. At the time of writing this Thesis, the ITS 2 is the largest-scale application of MAPS in a high-energy physics experiment.

The ITS 2 brought a plethora of improvements: i) a new beryllium beam pipe with an outer radius reduced from 28 mm to 18 mm allows for an innermost detector layer closer to the interaction point, from 39 mm to 22.4 mm; ii) an increased granularity for all layers, which are now silicon pixel detectors with a cell size of $29.24\text{ }\mu\text{m} \times 26.88\text{ }\mu\text{m}$; iii) the number of layers for the inner barrel was increased from two to three, raising the total number of layers from six to seven; iv) the material budget was reduced to $0.36\% X_0$ ($1.10\% X_0$) per layer for the innermost (outer) layers. A schematic view of the ITS 2 is presented in Fig. 3.4, while the main layout parameters are summarised in Table 3.1.

Table 3.1: Main layout parameters of the new ITS2. Table taken from Ref. [2].

Layer no.	Average radius (mm)	Stave length (mm)	No. of staves	No. of HICs/stave	Total no. of chips
0	23	271	12	1	108
1	31	271	16	1	144
2	39	271	20	1	180
3	196	844	24	8	2688
4	245	844	30	8	3360
5	344	1478	42	14	8232
6	393	1478	48	14	9408

3.2.3 Time Projection Chamber

The Time Projection Chamber (TPC) is the main tracking detector of the ALICE experiment, and is designed to provide particle identification via dE/dx of charged particles on a track-by-track basis up to $p_T \sim 1\text{ GeV}/c$ and precise momentum measurements. The TPC is a large cylindrical detector with a length and outer diameter of about 5 m, resulting in a volume of 88 m^3 filled with a gas mixture of Ne-CO₂-N₂ (90-10-5). The choice of a neon-based gas mixture in place of an argon-based one, used during the LHC Run 2 data-taking period to guarantee the stability of the readout chambers [18], was made to reduce the space-charge distortions in the drift volume. The higher ion mobility of the Ne-based mixture compared to similar Ar-based mixtures directly reduces the magnitude of the space-charge distortions

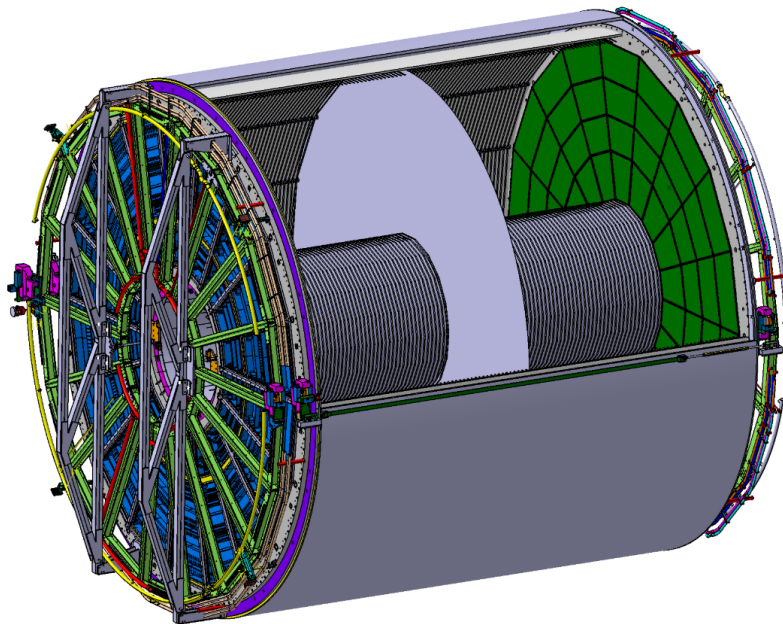


Figure 3.5: Schematic view of the ALICE TPC. Figure taken from Ref. [2].

by nearly a factor of two [19]. The TPC covers a symmetric pseudorapidity interval around midrapidity ($|\eta| < 0.9$) at full azimuth. The field cage has a high-voltage (100 kV) electrode in its center, which divides the active volume into two halves. The inner diameter of the central field cage drum is 114 cm, providing the necessary space for the installation of the ITS. Each of the two endplates houses 18 inner and outer readout chambers (IROCs and OROCs), which are arranged into pairs to form 18 equal azimuthal sectors.

During Runs 1 and 2, the readout chambers were based on MWPCs, which have to be operated with an active ion gating grid in order to prevent the ions produced in the amplification region from reaching the active drift volume, which could lead to space-charge distortions. The ambitious physics program of the ALICE experiment for Run 3 requires the elimination of the intrinsic trigger rate limitation of about 3 kHz of the original MWPC-based TPC, imposed by the operation of the active ion gating grid.

Operating the TPC at a collision rate of 50 kHz implies that on average five collision events pile up within the TPC readout time window of about $\sim 100 \mu\text{s}$. This excludes triggered operation and defines the need for continuous readout, requiring the exploitation of gas amplification techniques capable of providing sufficient ion blocking without an active gate. At the same time, the readout system must ensure that the dE/dx resolution of the TPC is preserved.

GEMs represent a valid solution to overcome the limitations of MWPCs. Sufficient ion blocking can be achieved by stacking four GEM foils using standard (S, 140 μm) and large (LP, 250 μm) hole pitch in an S-LP-LP-S configuration and by adjusting the gain share among the four layers. The latter optimisation allows for efficiently blocking the ions, most of which are produced in the last amplification step, i.e., in the layer closest to the readout pad. A careful choice of hole patterns is made to avoid the accidental alignment of holes in subsequent layers.

Thanks to this design, the detector is capable of satisfying the requirements for Run 3 operation, with an ion backflow below 2% and a local energy resolution at the ^{55}Fe -peak below 14% [20].

3.2.4 Time-of-Flight

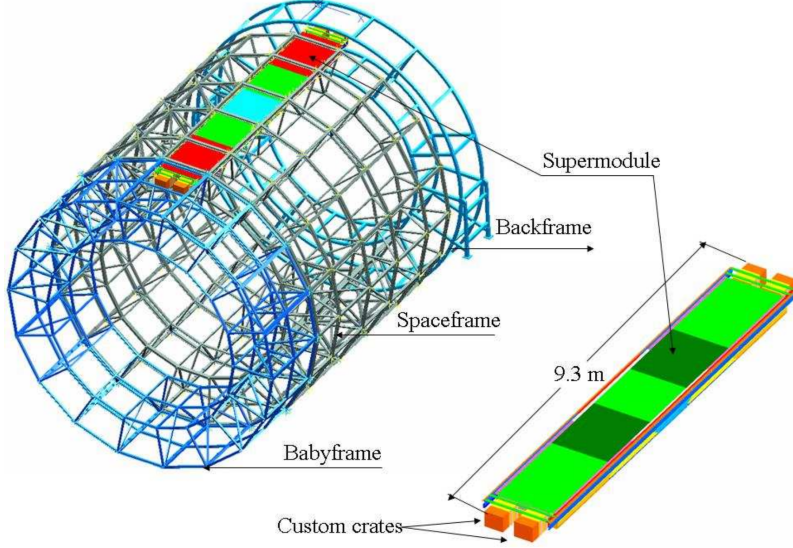


Figure 3.6: Schematic view of the ALICE TOF. Figure taken from Ref. [21].

The Time-of-Flight (TOF) detector is a large area detector covering the central pseudo-rapidity region ($|\eta| < 0.9$), extending from an inner radius of 370 cm to an external one of 399 cm. Its main purpose is the particle identification in the intermediate momentum range, achieving a π/K and K/p separation better than 3 times the time-of-flight resolution up to a momentum of about $2.5 \text{ GeV}/c$ for pions, and up to $4 \text{ GeV}/c$ for protons. The TOF detector is built with a modular structure corresponding to 18 sectors in φ and five modules along the beam direction. It is based on Multi-gap Resistive Plate Chambers (MRPCs) [22], which are capable of providing a time resolution of about 40 ps [1]. The gas mixture used in the MRPCs is $\text{C}_2\text{H}_2\text{F}_4(90\%)$, $\text{i-C}_4\text{H}_{10}(10\%)$, $\text{SF}_6(5\%)$, which proved to be a good solution as no significant ageing effects were observed after 3.5 times the dose foreseen in the first 10 years of operation.

Together with the ITS and TPC, the TOF is the detector in charge of providing event-by-event identification of large samples of pions, kaons, and protons. The mass of a given particle is estimated from the measurement of its time-of-flight:

$$m = p \cdot \sqrt{\left(\frac{t_{\text{flight}}}{L}\right)^2 - 1} \quad , \quad (3.1)$$

where p is the particle's momentum, measured from the curvature of the track trajectory, t_{flight} is the time-of-flight, and L is the track length. The time-of-flight is evaluated as the difference between the time of arrival of the particle at the TOF

(t_{hit}) and the time of the collision (t_0), estimated using a timing signal from the FT0 detector: $t_{\text{flight}} = t_{\text{hit}} - t_0$.

3.2.5 Fast Interaction Trigger

The Fast Interaction Trigger (FIT) serves as the main forward trigger, luminometer, and interaction-time detector. It also provides an initial indication of the vertex position and is used to determine the multiplicity, centrality, and reaction plane of heavy-ion collisions. The FIT consists of five distinct detector stations, positioned at different locations along the beam line: the FT0 (-A and -C), the FV0, and the FDD (-A and -C). An illustration of the FIT is shown in Fig. 3.7.

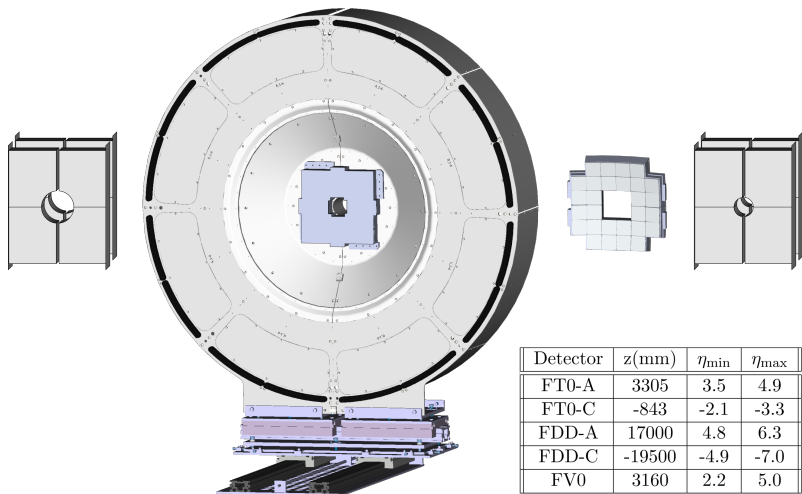


Figure 3.7: View of the FIT detectors illustrating the relative sizes of each component. From left to right, the FDD-A, FT0-A, FV0, FT0-C, and FDD-C are shown. The FT0-A and FV0 systems have a common mechanical support: the former is the small quadrangular structure in the centre of the large, circular FV0 support. The inset table lists the distance from the interaction point and the pseudorapidity coverage for each component. Figure taken from Ref. [2].

FT0

The FT0 is made of two arrays of quartz Cherenkov radiators, FT0-A and FT0-C, coupled to MicroChannel Plate-based photomultipliers (MCP). Its main task is to determine the vertex position with an accuracy of a few centimetres, and to provide the interaction time with the precision needed by the TOF system for event-by-event particle identification. An excellent time resolution (< 50 ps) is therefore required. The FT0-A is located at 3.3 m from the nominal interaction point, while the FT0-C is only 84 cm from the interaction point. To provide a reliable indication of the time of a collision, the FT0-C has a convex shape, to ensure that each of the 112 quartz radiators is positioned at a distance of 84 cm from the nominal interaction point. On the contrary, the FT0-A is characterised by a planar geometry, made of 96 quartz radiators. To achieve the best possible timing resolution, the signal

path from each MCP anode to the front-end electronics has the same length. The intrinsic time resolution of each quadrant is $\sigma_t \sim 13$ ps

FV0

The FV0 is a large, segmented scintillator disk. It achieves a single MIP time resolution of about 200 ps with a very uniform response across the entire detection surface thanks to its light collection scheme, shown in Fig. 3.8. The active element of FV0 is a 4 cm-thick plastic scintillator divided into five concentric rings of equal pseudorapidity coverage. The outer diameter of the largest ring is 144 cm and the inner diameter of the smallest is 8 cm. The four inner rings are subdivided into eight sectors of 45 degrees each, while the outermost ring, due to its large area, has 16 sectors. A grid of equal-length fibers is connected to the back side of the scintillator, where they are attached to the photomultiplier tubes (PMTs). Each sector is read out by an independent PMT to provide a minimum bias and multiplicity trigger, when coupled to the FT0 information.



Figure 3.8: Photograph of one half of the FV0 detector. Figure taken from Ref. [2].

FDD

The FDD is made of two similar arrays, FDD-A and FDD-C, surrounding the beam pipe on opposite sides of the nominal interaction point, and consisting of eight rectangular scintillator pads each, arranged into two overlapping layers of four sectors. A quadrant was removed from the innermost corner of each scintillator plate to allow for the passage of the beam pipe. Since the FDD covers a large pseudorapidity interval, and is sensitive to the presence of even a single MIP, it is an ideal system to tag interactions characterised by large rapidity gaps as those from photon-induced ultra-peripheral collisions or diffractive processes.

Bibliography

- [1] **ALICE** Collaboration, K. Aamodt *et al.*, “The ALICE experiment at the CERN LHC”, *JINST* **3** (2008) S08002.
- [2] **ALICE** Collaboration, “ALICE upgrades during the LHC Long Shutdown 2”, [arXiv:2302.01238 \[physics.ins-det\]](https://arxiv.org/abs/2302.01238).
- [3] “LHC Machine”, *JINST* **3** (2008) S08001.
- [4] S. Myers, “The LEP collider, from design to approval and commissioning”,.
- [5] E. Lopienska, “The CERN accelerator complex, layout in 2022. Complexe des accélérateurs du CERN en janvier 2022”,.
<https://cds.cern.ch/record/2800984>. General Photo.
- [6] **ATLAS** Collaboration, G. Aad *et al.*, “Observation of a new particle in the search for the Standard Model Higgs boson with the ATLAS detector at the LHC”, *Phys. Lett. B* **716** (2012) 1–29, [arXiv:1207.7214 \[hep-ex\]](https://arxiv.org/abs/1207.7214).
- [7] **CMS** Collaboration, S. Chatrchyan *et al.*, “Observation of a New Boson at a Mass of 125 GeV with the CMS Experiment at the LHC”, *Phys. Lett. B* **716** (2012) 30–61, [arXiv:1207.7235 \[hep-ex\]](https://arxiv.org/abs/1207.7235).
- [8] **ALICE** Collaboration, “ALICE Figure.”
<https://alice-figure.web.cern.ch/>.
- [9] F. Sauli, “GEM: A new concept for electron amplification in gas detectors”, *Nucl. Instrum. Meth. A* **386** (1997) 531–534.
- [10] Apache Arrow, “Apache Arrow, a cross-language development platform for in-memory analytics.” <https://arrow.apache.org/>.
- [11] R. Brun and F. Rademakers, “ROOT: An object oriented data analysis framework”, *Nucl. Instrum. Meth. A* **389** (1997) 81–86.
- [12] **ALICE** Collaboration, G. Aglieri Rinella, “The ALPIDE pixel sensor chip for the upgrade of the ALICE Inner Tracking System”, *Nucl. Instrum. Meth. A* **845** (2017) 583–587.
- [13] W. Snoeys, “CMOS monolithic active pixel sensors for high energy physics”, *Nucl. Instrum. Meth. A* **765** (2014) 167–171.

- [14] S. Senyukov, J. Baudot, A. Besson, G. Claus, L. Cousin, A. Dorokhov, W. Dulinski, M. Goffe, C. Hu-Guo, and M. Winter, “Charged particle detection performances of CMOS pixel sensors produced in a $0.18\mu\text{m}$ process with a high resistivity epitaxial layer”, *Nucl. Instrum. Meth. A* **730** (2013) 115–118, arXiv:1301.0515 [physics.ins-det].
- [15] CMS Collaboration, V. Karimäki, “The CMS tracker system project: Technical Design Report”,.
- [16] G. Aad *et al.*, “ATLAS pixel detector electronics and sensors”, *JINST* **3** (2008) P07007.
- [17] LHCb Collaboration, I. Bediaga, “LHCb VELO Upgrade Technical Design Report”,.
- [18] ALICE Collaboration, C. Lippmann, “Upgrade of the ALICE Time Projection Chamber”,.
- [19] A. Deisting, C. Garabatos, A. Szabo, and D. Vranic, “Measurements of ion mobility in argon and neon based gas mixtures”, *Nucl. Instrum. Meth. A* **845** (2017) 215–217, arXiv:1603.07638 [physics.ins-det].
- [20] ALICE TPC Collaboration, J. Adolfsson *et al.*, “The upgrade of the ALICE TPC with GEMs and continuous readout”, *JINST* **16** (2021) P03022, arXiv:2012.09518 [physics.ins-det].
- [21] ALICE Collaboration, B. B. Abelev *et al.*, “Performance of the ALICE Experiment at the CERN LHC”, *Int. J. Mod. Phys. A* **29** (2014) 1430044, arXiv:1402.4476 [nucl-ex].
- [22] Y. Wang and Y. Yu, “Multigap Resistive Plate Chambers for Time of Flight Applications”, *Appl. Sciences* **11** (2020) 111.